SCIENTIFIC REPORTS

OPEN

SUBJECT AREAS:
BATTERIES
ELECTROCHEMISTRY

Received
23 July 2014

Accepted
31 October 2014

Published
20 November 2014

Correspondence and requests for materials should be addressed to H.R.B. (hrbyon@riken.jp)

A structured three-dimensional polymer electrolyte with enlarged active reaction zone for Li–O_2 batteries

Nadège Bonnet-Mercier[1], Raymond A. Wong[1,2], Morgan L. Thomas[1], Arghya Dutta[1], Keisuke Yamanaka[3], Chihiro Yogi[3], Toshiaki Ohta[3] & Hye Ryung Byon[1]

[1]Byon Initiative Research Unit (IRU), RIKEN, Wako, Saitama 351-0198, Japan, [2]Department of Energy Sciences, Tokyo Institute of Technology, 4259 Nagatsuta-cho, Midori-ku, Yokohama 226-8502, Japan, [3]Synchrotron Radiation Center, Ritsumeikan University, Kusatsu, Shiga 525-8577, Japan.

The application of conventional solid polymer electrolyte (SPE) to lithium-oxygen (Li–O_2) batteries has suffered from a limited active reaction zone due to thick SPE and subsequent lack of O_2 gas diffusion route in the positive electrode. Here we present a new design for a three-dimensional (3-D) SPE structure, incorporating a carbon nanotube (CNT) electrode, adapted for a gas-based energy storage system. The void spaces in the porous CNT/SPE film allow an increased depth of diffusion of O_2 gas, providing an enlarged active reaction zone where Li^+ ions, O_2 gas, and electrons can interact. Furthermore, the thin SPE layer along the CNT, forming the core/shell nanostructure, aids in the smooth electron transfer when O_2 gas approaches the CNT surface. Therefore, the 3-D CNT/SPE electrode structure enhances the capacity in the SPE-based Li–O_2 cell. However, intrinsic instability of poly(ethylene oxide) (PEO) of the SPE matrix to superoxide ($O_2^{\cdot-}$) and high voltage gives rise to severe side reactions, convincing us of the need for development of a more stable electrolyte for use in this CNT/SPE design.

The lithium-oxygen (Li–O_2) battery has been extensively investigated as one of the promising future energy storage technologies requiring low cost and high gravimetric energy density[1–3]. Notably, based on excess Li^+ ion supplied from the metallic Li negative electrode and a continuous flux of O_2 gas through positive electrode, the Li–O_2 electrochemical reaction ($2Li^+ + O_2(g) + 2e^- \leftrightarrow Li_2O_2(s)$) renders a remarkable energy density (ca. 3 kWh kg^{-1}_{cell}) in a non-aqueous electrolyte[1,2]. However, the concept of combining metallic Li and O_2 gas leads to potential risks of fire and explosion, in particular, when a flammable liquid electrolyte is used. Therefore, a non-flammable, solid-state and soft medium, such as a solid polymer electrolyte and gel polymer electrolyte, can be considered as a promising alternative. Furthermore, the dense and thick solid polymer electrolyte (SPE) is expected to suppress O_2 crossover to the metallic Li, owing to the low gas solubility in the SPE. Despite these advantages, however, there have been only a few reports demonstrating SPE-based Li–O_2 cells[4–7]. One of the main reasons is the absence of an appropriate SPE structure adapted for a system including a gaseous active material. Namely, the conventional film SPE, which is either sandwiched in between the negative and positive electrodes or blended with the positive electrode material, cannot favorably serve for the O_2 gas diffusion *in the positive electrode*, due to the abovementioned reason. As a result, the active reaction zone, where the O_2 gas, Li^+ ion and electron can interact, is restricted to the topmost surface of the electrode/SPE boundary, which forms a limited two-dimensional (2-D) reaction zone (Figure 1a). To compensate for this, most SPE-based Li–O_2 cells were fabricated with thin and large-area carbon electrodes to deliver acceptable capacity[6,7]. Such a lateral expansion, however, is not very suitable for a viable storage device. Therefore, an improved SPE structure, designed specifically for a cell with gaseous active material should have a large active reaction zone along the longitudinal axis of the electrode (Figure 1b), which can be achieved by implementation of a O_2 diffusion path (voids) in the longitudinal direction and also a suitable electrode surface area. In addition, the SPE formed in close proximity to the electrode should be reasonably thin to aid in the smooth electron transfer to the O_2 gas. The close physical connection of electrode materials is also of importance to circumvent electrical losses when the sufficient O_2 diffusion paths are created.

Here we present a three-dimensional (3-D) active reaction zone using a newly designed SPE architecture for the Li–O_2 cell. The active reaction zone is established by a thin coating of carbon nanotube (CNT) with SPE and its integration into a 3-D structure incorporating sufficient void spaces. This can be achieved by soft permeation of

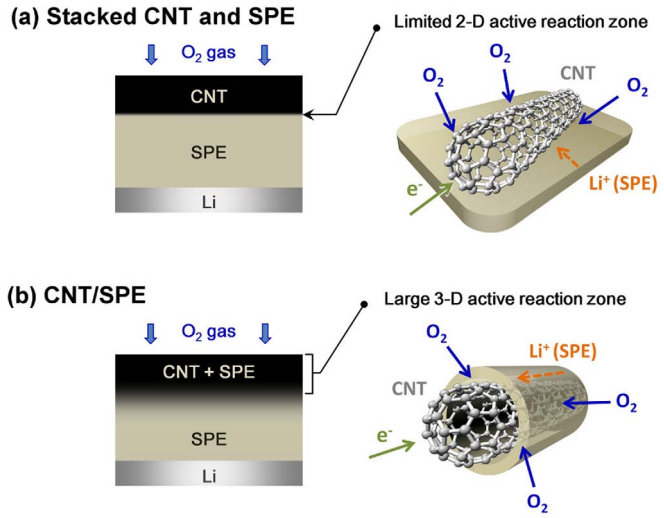

Figure 1 | Schematic illustrations of (a) limited 2-D active reaction zone in conventional CNT and SPE sandwiched structure and (b) enlarged 3-D active reaction zone in 3-D CNT/SPE architecture.

SPE into a 3-D CNT film using a hot-pressing technique. The resultant CNT/SPE is composed of a CNT core and tens of nanometers thick SPE shell, which is distributed in a ~30 μm depth of CNT electrode. The CNT/SPE-based Li–O_2 cell delivers higher capacity than those with the limited active reaction zones. However, for cycling, we observe severe side reactions, mostly arising from decomposition of the SPE matrix of poly(ethylene) oxide (PEO). This implies that the glycol ether-based electrolyte is poorly suited to the Li–O_2 cell.

Results

Fabrication of CNT/PEO-based SPE. The SPE-incorporated CNT electrode was fabricated via two steps: 1) preparation of free-standing CNT and PEO-based SPE films and 2) integration of SPE into the CNT using a hot-press technique (Figure 2a–c, see Methods for details). The binder-free CNT framework, prepared via vacuum filtration as described in our previous reports[8] (Figure 2a top), has a 3-D structure with a BET surface area of ~102 $m^2 g^{-1}$ and a pore (void) size of ~104 nm (Figure 2d). Typical thickness and mass of the CNT film we used are 50–60 μm and ~2 mg, respectively. The PEO-based SPE film was separately prepared under solvent-free and dry conditions. A mixture of precursors, PEO, lithium bis (trifluoromethanesulfonyl) imide (LiTFSI) with a molar ratio of EO/Li = 20, and a nanosized SiO_2 ceramic filler additive, was blended using a ball mill then processed by hot pressing. The resultant ~200 μm thick PEO-based film, more accurately referred to as $P(EO)_{20}$LiTFSI, is homogeneous, flexible and translucent (Figure 2a bottom) with a very low BET surface area of ~0.74 $m^2 g^{-1}$ and no clear trend of pore size distribution (Figure 2e). The film surface is flat and consists of domains with dimension of hundreds of nanometers (Figure S1). The physicochemical properties of the $P(EO)_{20}$LiTFSI in terms of melting temperature, ionic conductivity, and interfacial resistance are suitable for utilization of the

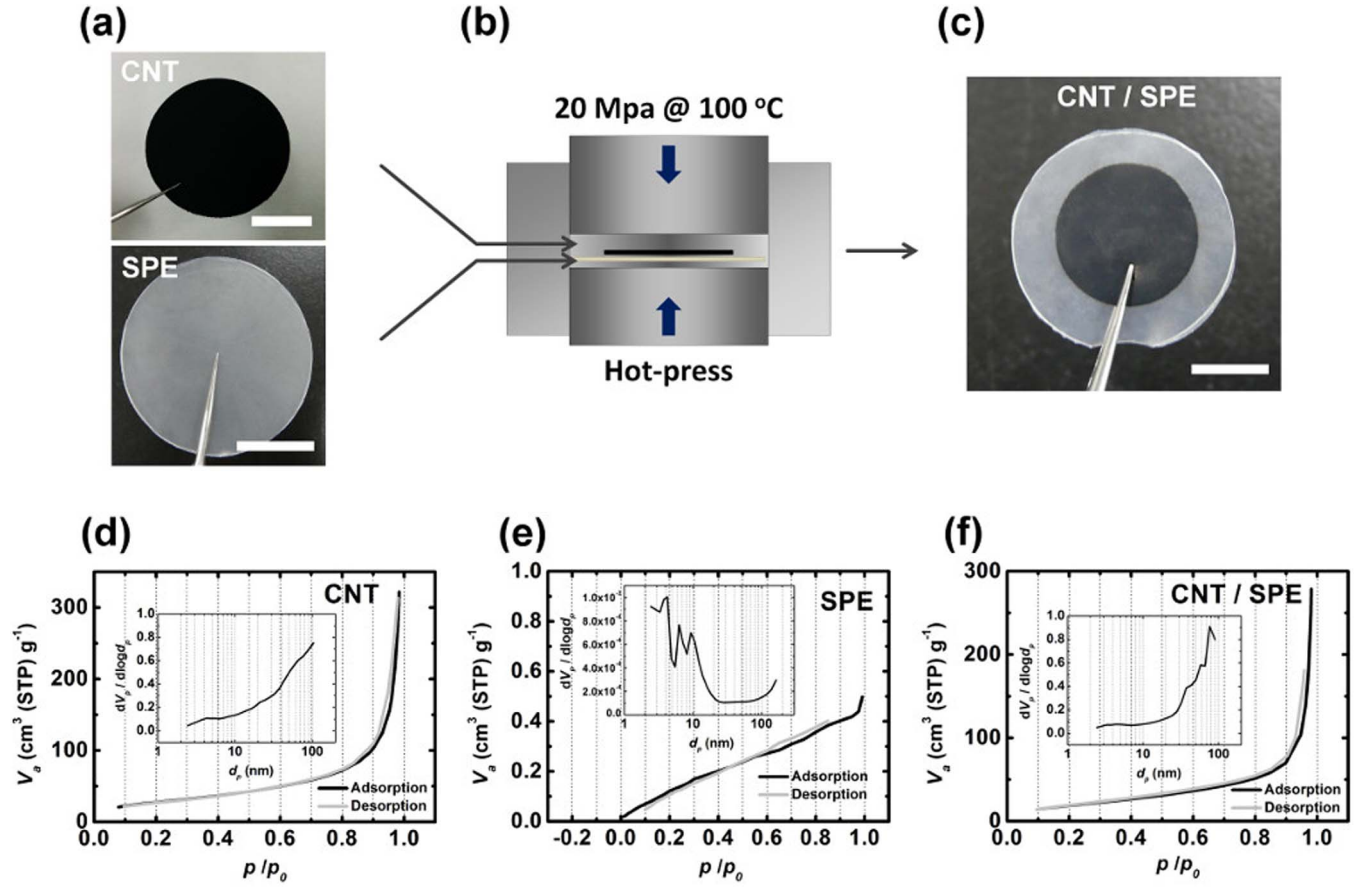

Figure 2 | Optical images and schematic view of preparation of 3-D CNT/SPE and N_2 adsorption-desorption isotherms. (a) Optical images of binder-free CNT films (top) and PEO-based SPE (bottom). The scale bars are 5 and 50 mm, respectively. (b) Schematic view of hot-pressing step of CNT and SPE films. (c) Optical image of complete CNT/SPE. The scale bar is 5 mm. (d–f) N_2 adsorption-desorption isotherms of (d) CNT film, (e) SPE and (f) CNT/SPE. The insets are the corresponding pore size distribution estimated by Barrett-Joyner-Halenda (BJH) method.

SPE in metallic Li/Li-ion based batteries. The heating profile observed in differential scanning calorimetry (DSC) in Figure S2a exhibits a glass transition (T_g) at −40°C and a melting point at 55°C. The ionic conductivity steeply increases close to the melting temperature as the crystalline to amorphous phase transition of PEO promotes the diffusion of Li^+[9]. Figure S2b demonstrates the ionic conductivity of $P(EO)_{20}LiTFSI$, which approaches 3.2×10^{-4} S cm^{-1} at 55°C. The stability of $P(EO)_{20}LiTFSI$ is also improved with increasing temperature in the presence of the metallic Li electrode. At 55°C, the interfacial resistance is an estimated ~140 Ω as shown in Figure S2c[10]. The ionic conductivity and interfacial resistance are comparable to those of typical PEO-based SPEs reported previously[11–13].

In the next step, the as-prepared PEO-based SPE and CNT films were integrated by hot pressing at 100°C for 10 min (Figure 2b). The CNT and SPE films were strongly fused through permeation of the melted $P(EO)_{20}LiTFSI$ film into the CNT at a pressure of 20 MPa followed by solidification during cooling. In the bulk, the complete CNT/SPE film encompasses the original CNT film intact without any structural deterioration (Figure 2c). In addition, the CNT/SPE maintains a reasonable surface area of ~75 m^2 g^{-1} with respect to the CNT mass and a pore size of ~75 nm (Figure 2f).

The SPE structure within the CNT/SPE can be further clarified using micron and nanometer-scaled imaging tools. The top-view scanning electron microscopy (SEM) images in Figure 3a and Figure S3a–b show the 3-D network structure of the CNT film. The CNTs are randomly connected within the film and the void spaces are preserved even after integration with the SPE (Figure 3b and Figure S3c–d). Atomic force microscopy (AFM) images with topography and phase modes in Figure 3c–d and Figure S4 demonstrate the core/shell structure of CNT/SPE. The clear contour of an inner and an outer layer, which is not observed in the absence of SPE (Figure S5), reflects the 5–40 nm thin coating of SPE on the CNT. Such a limited polymer layer cannot disturb the total electrical conductivity of the film surface. The sheet resistivity of CNT/SPE film, measured by four-probe technique, is ~1.6 Ω cm, which is comparable to that of the CNT-only film having ~1.3 Ω cm. More importantly, in the Li–O_2 cell, the core/shell structure of CNT/SPE in the film can provide a large active reaction zone. The 3-D conducting CNT network can rapidly transport the electrons across the film. The thinly covered SPE shell can supply the Li^+ ion along the CNT. The O_2 gas can diffuse to the inside of the CNT/SPE film via the void spaces and be involved in the Li–O_2 reaction close to the CNT/SPE structure surface. The advantages of this structure for the Li–O_2 cell are depicted in Figure 1b.

Such a 3-D SPE structure is retained longitudinally in bulk. The cross-sectional SEM image of the CNT/SPE film in Figure 3e displays two different layers: a top layer comprised of a ~50 μm thick 3-D CNT film covered with SPE, and bottom layer comprised of solely SPE of 150 μm thickness. The top layer shows a gradient of SPE concentration, where the void spaces within the CNT film become filled with higher proportion of the SPE with increasing depth. As a result, the upper part (to ~30 μm depth) preserves the active reaction zone where appreciable 3-D structure is present with the existence of sufficient void spaces (Figure 3f) while the lower part contains a higher concentration of SPE (Figure 3g) thus restricting the O_2 gas diffusion. When applied to the Li–O_2 battery with a metallic Li negative electrode, the bulk SPE layer at bottom separates the CNT/SPE part in the positive electrode from the Li with inhibition of electrical shorts.

Electrochemical performance and chemical identification of discharge and recharge products using CNT/PEO-based SPE for Li–O_2 cell. This CNT/SPE can be utilized for the Li–O_2 cell requiring a large active reaction zone for introduction of O_2 gas. The SPE-based Li–O_2 cell was examined at 55°C to endow the SPE with high ionic conductivity. The voltage profile of the CNT/SPE cell at a current rate

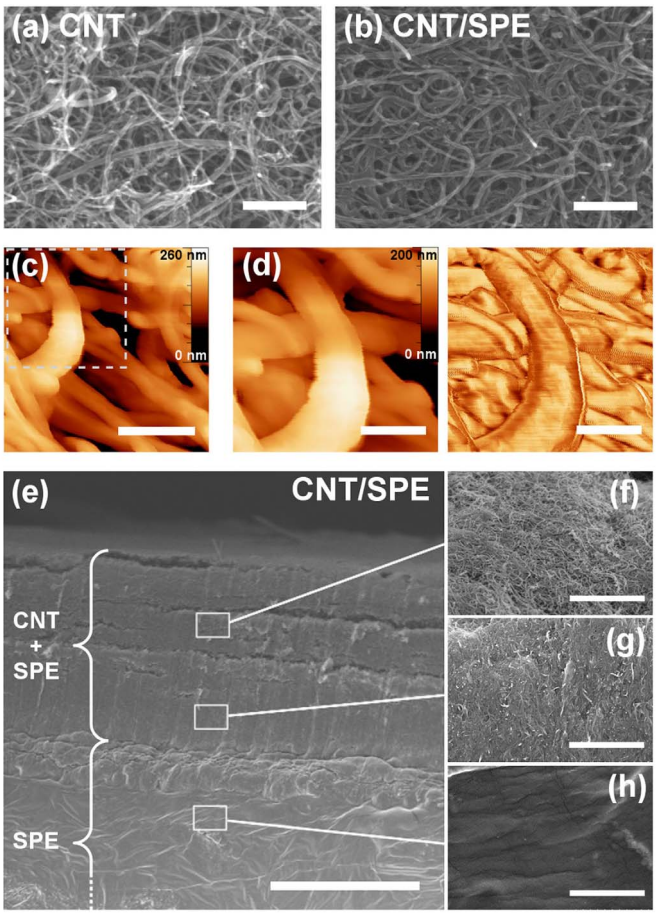

Figure 3 | Top and cross-sectional views of CNT and CNT/SPE. (a–b) Top-view SEM image of (a) CNT only and (b) CNT/SPE film. The scale bars are 500 nm. (c–d) AFM images of CNT/SPE surface. (d) is high-magnification topography (left) and phase (right) images of dashed square area in (c). The scale bars are (c) 300 nm and (d) 150 nm. The color bars on the right top of the topography images indicate the z-axis scale. (e–h) Cross-sectional SEM images of CNT/SPE. (f–h) are high-magnification images of the solid rectangular boxes in (e) for (f) top, (g) middle, and (h) bottom layers. The scale bars are (e) 50 μm and (f–h) 3 μm.

of 0.05 mA cm^{-2} in Figure 4a exhibits a discharge plateau of ~2.7 V (referred to Li^+/Li) for the 1st discharge (1DC) and recharge voltage increasing up to 4.25–4.5 V for the 1st recharge (1RC). The discharge capacity of the CNT/SPE Li–O_2 cell approaches 300–500 mAh g^{-1}_{CNT} for deep depth of discharge (a cutoff voltage of 2.0 V) on the basis of a ~2 mg CNT electrode, which is notably higher in comparison with that in the absence of O_2 gas (Figure S6). In addition, the CNT/SPE cell has greater discharge capacity than the CNT cell with a conventional SPE structure (Figure 4a). The sandwiched structure of CNT and SPE films provides a low capacity of ~125 mAh g^{-1}_{CNT} due to the restricted active reaction zone. Post heating of the sandwiched layers at 100°C for 30 min enhances the capacity up to ~200 mAh g^{-1}_{CNT} but still a lower capacity than the CNT/SPE. It is also noted that, despite the enlarged active reaction zone, the CNT/SPE cell has ~4 fold lower capacity than the glyme electrolyte-based Li–O_2 cell such as tetraethylene glycol dimethyl ether (tetraglyme) containing 0.5 M LiTFSI (Figure S7). It may be attributed to (1) dead reaction zone at the bottom of CNT film, (2) two orders of magnitude lower ionic conductivity of SPE compared to the liquid electrolyte and (3) high yield of side reaction arising from the PEO (see below).

The improved active reaction space, however, also provides a greater opportunity for chronic side reactions in the Li–O_2 cells,

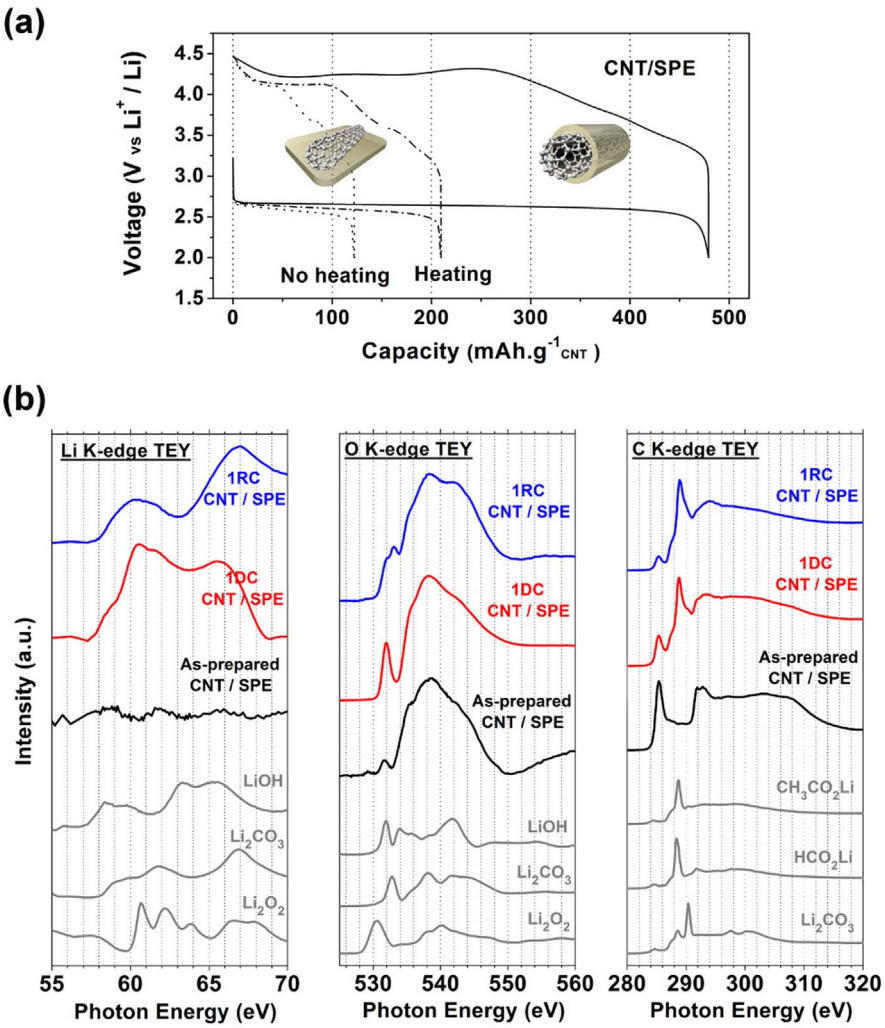

Figure 4 | Electrochemical performance of Li–O_2 cell and chemical identification of discharge and recharge products for CNT/SPE. (a) The 1st-cycled discharge-recharge curves of 3-D CNT/SPE (solid line), conventional CNT and SPE sandwiched structure with (dashed dot line) and without (dot line) heat treatment. The current rate is 0.05 mA cm^{-2} and operating temperature is 55°C. (b) XANES spectra with the total electron yield (TEY) mode in Li, O, and C K edge (from left to right). The black, red, and blue spectra are as-prepared, 1DC, and 1RC CNT/SPE, respectively. The gray spectra are standard samples of lithium compounds acquired from commercial powders. The *n*DC and *n*RC denote *n*-times cycled electrodes at the end of discharge and recharge, respectively.

which results in deposition of side products. Figure 4b exhibits Li, O, and C K-edge X-ray absorption near edge structure (XANES) spectra with the surface-sensitive total electron yield (TEY) mode. The 1DC and 1RC electrode spectra can be directly compared to those of as-prepared CNT/SPE and standard powder samples of lithium compounds to assist in chemical identification of newly formed products. For the 1DC CNT/SPE, the Li K-edge spectrum demonstrates the presence of both lithium peroxide (Li_2O_2) and lithium hydroxide (LiOH); the sharp peaks at 60.5 and 61.8 eV are correlated with the Li_2O_2 while the edge shoulder at 58.5 eV arises from the LiOH. The Li_2O_2 peak, however, cannot be observed in the O K-edge spectrum. The pronounced peak at 532 eV for the 1DC CNT/SPE is mostly attributed to the LiOH. This discrepancy can be accounted for by the different depth sensitivity for Li (~1 nm) and O (~10 nm) K-edge spectroscopy with the TEY mode. Namely, the Li_2O_2 exists on the topmost surface while the LiOH product is distributed in depth, which is further corroborated by the sole presence of LiOH in the bulk-sensitive fluorescence yield (FY) mode (Figure S8) and X-ray diffraction (XRD) pattern (Figure S9) although we cannot rule out the presence of amorphous Li_2O_2. Along with the LiOH, the lithium carboxylates, mostly lithium formate (HCO_2Li, see Figure S10), and lithium carbonate (Li_2CO_3) are also present. The C K-edge spectrum reveals an appreciable carboxylates-associated peak at 288.5 eV and Li_2CO_3-related small peak at 290.5 eV. All these side products are also present after the 1RC. In particular, the Li_2CO_3 and lithium carboxylates become greater. The O K-edge spectrum clearly exhibits a Li_2CO_3-associated peak at 533 eV. The C K-edge region displays a higher intensity of the lithium carboxylates-related peak relative to the π* band transition of CNT peak (~285.5 eV)[14], compared to that for the 1DC, which is also verified in the ^{1}H NMR spectra (Figure S10).

Discussion

The XANES results demonstrate the occurrence of acute side reaction rather than the ideal Li–O_2 electrochemical reaction. As a matter of fact, such side reactions are not very surprising in the Li–O_2 cell. The non-aqueous electrolyte is easily subject to parasitic side reaction through the nucleophilic attack from the superoxide radical ($O_2^{\cdot -}$) during discharge, and also for the greatly rising voltage during recharge[18,19]. The liquid ether-based glyme electrolyte, even though it is known to have higher tolerance for the $O_2^{\cdot -}$ than, for example, carbonate electrolytes, is also subject to side reactions upon cycling, and results in the precipitation of side products of lithium carbonates and lithium carboxylates[8,15,16]. Such formation of side products with

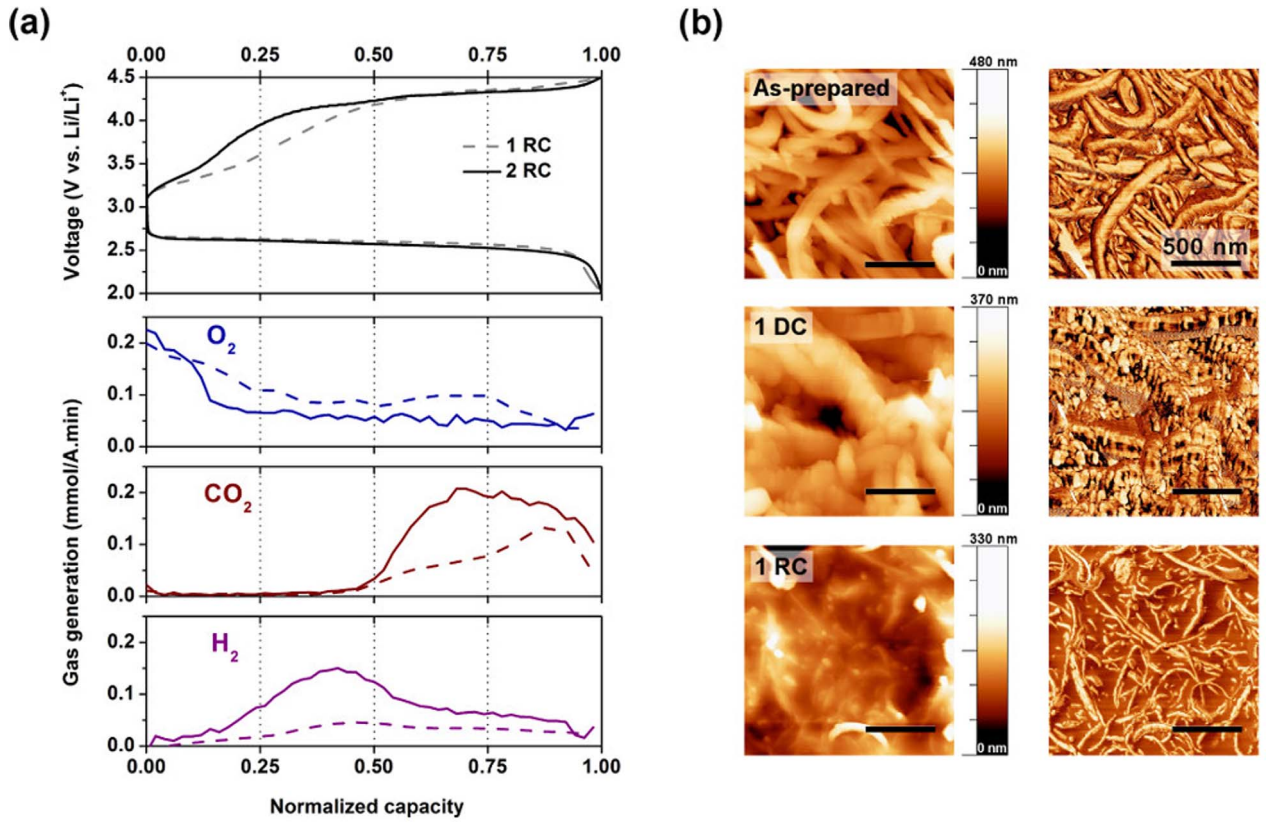

Figure 5 | *In situ* OEMS results for total 2 cycles and AFM images of CNT/SPE structure after 1DC and 1RC. (a) The gas evolution during the 1st (dashed lines) and 2nd (solid lines) recharge at a current rate of 0.05 mA cm^{-2} at 55°C. (b) Topography (left column) and phase (right column) AFM images of as-prepared, 1DC, and 1RC CNT/SPE (from top to bottom). The scale bars are 500 nm. The color bars indicate the z-axis scale of topography images.

the corresponding depletion of electrolyte is one of the most critical problems for the non-aqueous Li–O_2 cell[2]. However, the PEO-based SPE, which is also comprised of repeated ether moieties in a long chain in addition to alcohol termination, seems to undergo more severe side reactions as revealed by the substantial side products even during the 1st cycle. In addition, interestingly, the considerable amount of LiOH is not the typical side product for the glyme-based Li–O_2 cell. The possible origin of LiOH is generally considered to be due to either H_2O contamination[17] or metal oxide promoter in the presence of dehydrofluorination of poly(vinylidene fluoride) (PVdF) binder[18]. However, dry and inert conditions were maintained for the preparation of CNT/SPE and assembly/operation of CNT/SPE cells. In addition, all materials and cell components were almost completely dried. The PEO (T_m = 65°C) and LiTFSI were dried at 60 and 80°C, respectively, in a vacuum oven for 48 h[19,20]. When the LiTFSI was added to tetraglyme (which was pre-dried with with molecular sieves overnight), the H_2O content measured by Karl Fischer titration was less than 10 ppm, which demonstrated negligible H_2O in the LiTFSI. The SiO_2 nanofiller was typically dried at 60°C in a vacuum oven. This relatively low temperature might result in the introduction of trace H_2O. Therefore, we also examined further drying of SiO_2 nanofillers at 300°C for 48 h under vacuum. The 1DC XRD and XANES results still exhibited the existence of LiOH (Figure S11). Therefore, the complete drying of SiO_2 at 300°C might decrease the amount of LiOH but does not fully prevent the formation of LiOH. Besides, the CNT/SPE is binder free and no existence of metal oxide promoter, which completely excludes these possible side reactions to produce the LiOH analogous to the typical glyme-based Li–O_2 reaction[8].

This implies that the LiOH side product can be mostly formed by the severe decomposition of PEO-based SPE in the Li–O_2 cell. The intrinsic instability of the PEO matrix for the $O_2^{\cdot -}$ can be demonstrated by its dissociation during discharge. ^{1}H NMR spectra in Figure S12 reveal the appearance of a notable methyl ether ($-OCH_3$) peak at a chemical shift of 3.4 ppm after 1DC and 2nd-cycled discharge (2DC) at a low current rate (0.01 mA cm^{-2}). This result can arise from formation of peroxide radical moiety into the β carbon of ether backbone of the PEO via the nucleophile reaction with the $O_2^{\cdot -}$, followed by carbon-carbon bond scission (Figure S13)[15,19,21–25]. More importantly, the serious degradation of PEO is accompanied by the byproduct of H_2O and formates via hydrogen abstraction (see the proposed mechanism in Figure S13), which possibly affects the formation of high-yield LiOH and HCO_2Li via chemical reactions. In addition, upon recharge, the PEO matrix can be easily oxidized. Its oxidation resistivity is lower than that of glyme. Figure S14 shows linear sweep voltammetry (LSV) curves of PEO-based SPE and tetraglyme electrolyte under Ar atmosphere. For the PEO electrolyte, the oxidation becomes vigorous over 4.25 V, while it is appreciable only over 4.5 V for the tetraglyme electrolyte. The significant oxidation of PEO during recharge, therefore, induces not only the deposition of side products but also polymerization of the dissociated glycol polyether chains[15,26] as evidenced by disappearance of the methyl ether peak after the 1RC in the ^{1}H NMR spectrum (Figure S12).

The repeating of this complex process results in abundant side products and depletion of the electrolyte. The *in situ* online electrochemical mass spectroscopy (OEMS) result in Figure 5a exhibits the gas evolution for cycling. For the 1RC, the O_2 gas is released at the initial stage according to the oxidation of Li_2O_2 then the CO_2 gas evolution becomes great over 4.25 V due to the decomposition of Li_2CO_3 and HCO_2Li. It is reported that the LiOH itself does not contribute to evolve either O_2 or H_2 gas during oxidation[27]. Therefore, the O_2 evolution totally arises from the Li_2O_2 while its

portion (34% of the total charge) seems to be significant considering that the Li_2O_2 is observed only on the topmost surface of CNT/SPE in the XANES result (Figure 4b). We suppose that the Li_2O_2 is chemically transformed to LiOH during the preparation of the XANES measurement (at least 2–3 days) in the presence of H_2O byproduct that is trapped inside the CNT/SPE. On the contrary, the constantly flowing O_2 gas during discharge and consecutive measurement of OEMS with 6 h rest time after the discharge can reduce the chance of chemical transformation of Li_2O_2 prior to its electrochemical recharge. More interestingly, the successive OEMS result for the 2RC reveals a remarkable increase in the amount of H_2 followed by CO_2 as the recharge progresses. This gas-evolution behavior is also distinguished from that in a glyme-based Li–O_2 cell, providing a similar trend of O_2 and CO_2 gas evolution for both 1RC and 2RC (Figure S15). In particular, considerable H_2 gas evolution is only observed in the PEO, which reflects the huge hydrogen abstraction.

These severe side reactions disrupt the 3-D CNT/SPE structure. Figure 5b and Figure S16 show AFM topography and phase images of as-prepared, 1DC, and 1RC CNT/SPE film. After the 1DC, granular shaped products are formed along the CNT/SPE network, which disappear during the 1RC. More importantly, the CNT/SPE structure is degraded after the 1RC. The topography image shows the newly formed film on top, which covers the CNT networks. The thinner diameter network, shown in the phase image, than that for the as-prepared CNT/SPE is most likely due to elimination of the PEO-based SPE shell from the CNT. The degraded PEO shell can be polymerized, thus forming the thick film during the 1RC. This is also confirmed by the SEM images in Figure S17 where the gelified film layers inhomogeneously screen the CNT surfaces and void spaces after the 1RC. Furthermore, the repeated discharge-recharge cycles damage the CNT/SPE structure and deplete the PEO matrix, which eventually gives rise to cell failure (Figure S18). The disassembled cell after failure revealed the gelified product on the CNT side while the SPE-only bottom layer bridging the metallic Li is not visible to the naked eyes, causing an electrical short. Namely, rapid depletion occurs in the thick PEO matrix (~150 μm thick) once the degradation is propagated. Therefore, it is concluded that the PEO-based SPE is not applicable for the practical Li–O_2 cell. Although the glyme having the shorter ether chains has higher resistivity, this also can be rapidly degraded upon further cycling[15], thus the development of a more stable electrolyte is of significance to advance a practical Li–O_2 battery.

In summary, we have developed a 3-D SPE structure on a CNT framework aimed at a gas based energy storage system. A SPE thinly coated along the 3-D CNT electrode surface can maintain void spaces in the CNT film, which could allow gas introduction in depth into the CNT/SPE. In particular, the introduced gas can be smoothly involved in the electrochemical reaction by approaching the CNT surface with little hindrance from the SPE. As a representative example, such a 3-D CNT/SPE structure was applied for Li–O_2 cells, which demonstrated reasonable discharge capacities and voltage profiles for the initial cycle. This new design for an electrode/SPE is essential to achieve advanced batteries, which can be made feasible with development of a more stable SPE.

Methods

Preparation of PEO-based solid polymer electrolyte (SPE). The poly(ethylene oxide) (PEO) matrix was employed as a SPE matrix because its high stability to the metallic Li can suppress the growth of Li dendrites[10,28,29] and the repeated ether moieties are similar to the glyme that is commonly used. The PEO-based SPEs were prepared using ball-milling and hot-press methods under completely moisture- and solvent-free conditions. PEO (MW 6×10^5, $T_m = 65^\circ C$, Aldrich), lithium bis(trifluoromethanesulfonyl)imide (LiTFSI, 99.7% purity, Kanto Chemical Co.), and fumed SiO_2 nanoparticles (size < 7 nm, Aldrich) were dried at 60, 80 and 60°C (or 300°C using Büchi glass oven (B-585 Kugelrohr)), respectively, under vacuum for at least 48 h before use and mixed homogeneously with a ball mill (Fritsch Pulverisette 6). For the ball milling, the PEO and LiTFSI with an EO/Li molar ratio of 20 and 10 wt% SiO_2 were loaded into a ZrO_2 container with ZrO_2 balls (diameter = 5 mm) in an Ar-filled dry glove box (H_2O < 1 ppm and O_2 < 5 ppm, Kiyon/ALS). The additive SiO_2 was used to improve ionic conductivity, lithium interfacial stability, and mechanical strength[11–13,28,30–32]. The container was sealed air-tightly using an over pot system and ball milled at 450 rpm for 35 min (Fritsch Pulverisette 6). The mixture was then sandwiched between two Teflon sheets in the glove box and pressed using a hydraulic press (MTI YLJ-12T) at 100°C and 20 MPa for 10 min, which resulted in homogeneous, flexible, and semi-transparent SPEs with an average thickness of 200 ± 50 μm (Figure 2).

Preparation of CNT/SPE. Free-standing and binder-free CNT films (average thickness ≈ 70 μm) were prepared by vacuum filtration. 20 mg of CNT (97% purity, average diameter ≈ 20 nm, Applied Carbon Nano Technology Company) was immersed in 5 g of isopropanol and tip sonicated for 15 min in an ice bath. The CNT solution was then vacuum filtrated on a glass fiber filter paper (diameter ≈ 45 mm, GF/C, Whatman) and dried under vacuum at 60°C for at least 12 h. The completely dried CNT film was placed on the as-prepared SPE and covered by the Teflon (SPE side) and aluminum (CNT side) sheets. The hydraulic press was used to make the CNT/SPE at 100°C and 20 MPa for 10 min and the complete CNT/SPE was dried in a vacuum oven at 40°C for at least 12 h. The CNT/SPE films were cut with a diameter of 12 mm. The typical CNT mass was ~2 mg.

Assembly of Li–O_2 cells and galvanostatic measurements. All cell assemblies were carried out in an Ar-filled glove box. The custom-made Li–O_2 cells designed with Tomcell® and components were dried in the vacuum oven at 60°C overnight prior to transferring into the glove box. The Li–O_2 cells were assembled with a metallic Li disk (diameter ≈ 12 mm, Honjo) on a stainless steel plate as the negative electrode, CNT/SPE as the positive electrode/electrolyte, and stainless steel mesh in the Ar-filled glove box. The completely assembled cell containing an O_2 tank (40 mL volume capacity) was filled with dry O_2 gas (purity > 99.999%, Tomoe Shokai Co. Ltd.) by purging the O_2 gas at 100 sccm (standard cubic centimeter per minute) for 15 min. Galvanostatic discharge-recharge examinations were conducted using a constant temperature chamber (Isuzu seisakusho) with a set temperature of 55°C. After maintaining the open circuit voltage for 3 h, the galvanostatic measurements were examined in a voltage range of 2.0–4.5 V at a current rate of 0.05 mA cm^{-2}, unless otherwise mentioned, using a battery cycler (WonATech WBCS3000). All voltages were referred to Li^+/Li.

Characterization. The surface area and porosity was calculated by Brunauer-Emmett-Teller (BET) and Barrett-Joyner-Halenda (BJH) method, respectively, based on N_2 adsorption-desorption isotherms (BELSORP-mini II, BEL Japan Inc.). The CNT/SPEs examined were disassembled in the glove box after Ar gas purging into the cells and dried in a vacuum oven linked to the glove box at 40°C for at least 12 h without exposing them to air. The dried CNT/SPEs were conveyed using hermetic vessels. SEM images were attained from a Hitachi S-4800T with 5 kV accelerating voltage. AFM images were collected with a tapping mode from an Agilent 5500 AFM/SPM equipped in the Ar-filled glove box using silicon tips (radius < 7 nm, force constant ≈ 42 N m^{-1}, a frequency of 330 kHz, Agilent). The four-probe technique for measurement of film sheet resistivity was carried out using a NPS Sigma-5+ resistivity processor. O, C, and Li K-edge X-ray absorption near-edge structure (XANES) spectral measurements with the FY and TEY modes were performed at BL-2 in the SR center of Ritsumeikan University. All CNT/SPE samples and references of Li_2O_2 (99% purity, Kojundo Chemical Laboratory Co., Ltd), LiOH (98%, Sigma-Aldrich), Li_2CO_3 (99%, Nacalai Tesque Inc.), $HCO_2Li \cdot H_2O$ (98%, Sigma-Aldrich) and CH_3CO_2Li (>98%, Wako Chemicals) were loaded on a custom-made hermetic vacuum vessel in the glove box and directly transferred into the XANES chamber without air exposure. *In situ* and on-line gas analysis measurements were conducted using a home-made *in situ* online electrochemical mass spectroscopy (OEMS) and a custom-made cell (designed with Tomcell®). The OEMS setup is similar to existing reports by McCloskey *et al.*[33] using a 6-way,2-position gas chromatography valve. A LabVIEW interface allowed for the automated manipulation of valves and data collection from the pressure gauges and mass spectrometer. The response of the detector was calibrated with mixtures of gases (typically a series of 5 concentrations in the range 0.00–0.25 vol.% giving rise to a linear relationship between partial pressure and gas concentration) for O_2, CO_2 and H_2 in Ar. Mass flow controllers (Kofloc, Japan) were employed for the accurate preparation of calibration mixtures. The Li–O_2 OEMS cell had identical design to the general Li–O_2 cell except the upper headspace portion contained a considerably smaller volume to allow for high concentrations of gaseous products to form during recharge. The headspace volume of the cell was measured by comparison with a calibration for volume performed using a series of known volume samples loops (250 μL, 500 μL, 1 mL. 2 mL and 5 mL). A detailed description of this process is provided by McCloskey *et al.*[33] and is based on the observed pressure rise for each known volume. Galvanostatic discharge of the cell was performed in an incubator using a single channel battery cycler (WonATech WPG100e), with an O_2 flow of 10 sccm. During recharge, Ar was used as the diluent. Mass spectroscopy measurements were made periodically (typically 15 or 30 min), followed by a short period (1 min) of flushing Ar gas at 100 sccm through the cell to prevent carry-over of accumulated gas (e.g. O_2 and CO_2) to the next sample. Quantitative analysis was thus achieved by consideration of the headspace volume and gas composition.

1. Girishkumar, G., McCloskey, B., Luntz, A. C., Swanson, S. & Wilcke, W. Lithium−air battery: promise and challenges. *J. Phys. Chem. Lett.* **1**, 2193–2203 (2010).

2. Bruce, P. G., Freunberger, S. A., Hardwick, L. J. & Tarascon, J.-M. Li–O_2 and Li–S batteries with high energy storage. *Nature materials* **11**, 19–29 (2012).
3. Lu, Y.-C. *et al.* Lithium–oxygen batteries: bridging mechanistic understanding and battery performance. *Energy Environ. Sci.* **6**, 750–768 (2013).
4. Abraham, K. M. & Jiang, Z. A polymer electrolyte-based rechargeable lithium/oxygen battery. *J. Electrochemc. Soc.* **143**, 1–5 (1996).
5. Zhang, D., Li, R., Huang, T. & Yu, A. Novel composite polymer electrolyte for lithium air batteries. *J. Power Sources* **195**, 1202–1206 (2010).
6. Hassoun, J., Croce, F., Armand, M. & Scrosati, B. Investigation of the O_2 electrochemistry in a polymer electrolyte solid state cell. *Angew. Chem. Int. Ed.* **50**, 2999–3002 (2011).
7. Jung, K.-N., Lee, J.-I., Jung, J.-H., Shin, K.-H. & Lee, J.-W. A quasi-solid-state rechargeable lithium-oxygen battery based on a gel polymer electrolyte with an ionic liquid. *Chem. Commun.* **50**, 5458–5461 (2014).
8. Yilmaz, E., Yogi, C., Yamanaka, K., Ohta, T. & Byon, H. R. Promoting formation of noncrystalline Li_2O_2 in the Li–O_2 battery with RuO_2 nanoparticles. *Nano letters* **13**, 4679–4684 (2013).
9. Meyer, W. H. Polymer electrolytes for lithium-ion batteries. *Adv. Mater.* **10**, 439–448 (1999).
10. Zhang, T. *et al.* Li/polymer electrolyte/water stable lithium-conducting glass ceramics composite for lithium-air secondary batteries with an aqueous electrolyte. *J. Electrochemc. Soc.* **155**, A965–A969 (2008).
11. Borghini, M. C., Mastragostino, M., Passerini, S. & Scrosati, B. Electrochemical Properties of Polyethylene Oxide-Li[$(CF_3SO_2)_2N$]-Gamma-$LiAlO_2$ Composite Polymer Electrolytes. *J. Electrochemc. Soc.* **142**, 2118–2121 (1995).
12. Appetecchi, G. B. *et al.* Composite Polymer Electrolytes with Improved Lithium Metal Electrode Interfacial Properties: I. Elechtrochemical Properties of Dry PEO-LiX Systems. *J. Electrochemc. Soc.* **145**, 4126–4132 (1998).
13. Appetecchi, G. B. *et al.* Hot-pressed, dry, composite, PEO-based electrolyte membranes: I. Ionic conductivity characterization. *J. Power Sources* **114**, 105–112 (2003).
14. Medjo, R. E., Sendja, B. T., Mane, J. M. & Ateba, P. O. A study of carbon nanotube contamination by XANES spectroscopy. *Phys. Scr.* **80**, 045601 (2009).
15. Freunberger, S. A. *et al.* The lithium–oxygen battery with ether-based electrolytes. *Angew. Chem. Int. Ed.* **50**, 8609–8613 (2011).
16. Wen, R., Hong, M. & Byon, H. R. In situ AFM imaging of Li–O_2 electrochemical reaction on highly oriented pyrolytic graphite with ether-based electrolyte. *J. Am. Chem. Soc.* **135**, 10870–10876 (2013).
17. Guo, Z., Dong, X., Yuan, S., Wang, Y. & Xia, Y. Humidity effect on electrochemical performance of Li–O_2 batteries. *J. Power Sources* **264**, 1–7 (2014).
18. Black, R. *et al.* Screening for superoxide reactivity in Li–O_2 batteries: effect on Li_2O_2/LiOH crystallization. *J. Am. Chem. Soc.* **134**, 2902–2905 (2012).
19. Nasybulin, E. *et al.* Stability of polymer binders in Li–O_2 batteries. *J. Power Sources* **243**, 899–907 (2013).
20. Nasybulin, E. *et al.* Effects of electrolyte salts on the performance of Li–O_2 batteries. *J. Phys. Chem. C* **117**, 2635–2645 (2013).
21. Decker, C. & Marchal, J. Caractérisation de réactions primaires de dégradation oxydante au cours de l'autoxydation des polyoxyéthylènes à 25°C: Étude en solution aqueuse avec amorçage par radiolyse du solvant. VI. Polyoxyéthylène: Produits d'oxydation et schéma cinétique. *Die Makromolekulare Chemie* **166**, 155–178 (1973).
22. Yang, L., Heatley, F., Blease, T. G. & Thompson, R. I. G. A study of the mechanism of the oxidative thermal degradation of poly(ethylene oxide) and poly(propylene oxide) using H-1- and C-13-NMR. *Eur Polym J* **32**, 535–547 (1996).
23. Gallet, G., Carroccio, S., Rizzarelli, P. & Karlsson, S. Thermal degradation of poly(ethylene oxide-propylene oxide-ethylene oxide) triblock copolymer: comparative study by SEC/NMR, SEC/MALDI-TOF-MS and SPME/GC-MS. *Polymer* **43**, 1081–1094 (2002).
24. Dulog, V. L. & Storck, G. Die oxydation von polyepoxiden mit molekularem sauerstoff. *Die Makromolekulare Chemie* **91**, 50–73 (1966).
25. Mkhatresh, O. A. & Heatley, F. A study of the products and mechanism of the thermal oxidative degradation of poly(ethylene oxide) using H-1 and C-13 1-D and 2-D NMR. *Polym Int* **53**, 1336–1342 (2004).
26. Tsiouvaras, N., Meini, S., Buchberger, I. & Gasteiger, H. A. A novel on-line mass spectrometer design for the study of multiple charging cycles of a Li–O_2 battery. *J. Electrochemc. Soc.* **160**, A471–A477 (2013).
27. Meini, S. *et al.* Rechargeability of Li-air cathodes pre-filled with discharge products using an ether-based electrolyte solution: implications for cycle-life of Li-air cells. *Phys. Chem. Chem. Phys.* **15**, 11478–11493 (2013).
28. Croce, F., Appetecchi, G. B., Persi, L. & Scrosati, B. Nanocomposite polymer electrolytes for lithium batteries. *Nature* **394**, 456–458 (1998).
29. Zhang, T., Imanishi, N., Takeda, Y. & Yamamoto, O. Aqueous lithium/air rechargeable batteries. *Chem. Lett.* **40**, 668–674 (2011).
30. Scrosati, B., Croce, F. & Panero, S. Progress in lithium polymer battery R&D. *J. Power Sources* **100**, 93–100 (2001).
31. Li, Q. *et al.* Interface properties between a lithium metal electrode and a poly(ethylene oxide) based composite polymer electrolyte. *J. Power Sources* **94**, 201–205 (2001).
32. Li, Q. *et al.* Cycling perfomances and interfacial properties of a Li/PEO-Li$(CF_3SO_2)_2N$-ceramic filler/$LiNi_{0.8}Co_{0.2}O_2$ cell. *J. Power Sources* **97–98**, 795–797 (2001).
33. McCloskey, B. D., Bethune, D. S., Shelby, R. M., Girishkumar, G. & Luntz, A. C. Solvents' critical role in nonaqueous lithium–oxygen battery electrochemistry. *J. Phys. Chem. Lett.* **2**, 1161–1166 (2011).

Acknowledgments

This work was financially supported by RIKEN, JST ALCA program, and MEXT project for CRP (Proposal No. R1307 and R1329). The authors greatly thank Ms. Misun Hong and Dr. Rui Wen for assistance with AFM scanning.

Author contributions

N.B.M. and H.R.B. designed the experiments and N.B.M. and R.A.W. performed main experiments. M.L.T. and R.A.W. performed the OEMS analysis, A.D. measured the N_2 adsorption-desorption isotherm, and K.Y., C.Y. and T.O. conducted the XANES analysis. M.L.T., N.B.M. and H.R.B. discussed the dissociation mechanism of PEO. N.B.M. and H.R.B. wrote the manuscript and all authors discussed the results on the manuscript.

Additional information

Supplementary information accompanies this paper at http://www.nature.com/scientificreports

Competing financial interests: The authors declare no competing financial interests.

How to cite this article: Bonnet-Mercier, N. *et al.* A structured three-dimensional polymer electrolyte with enlarged active reaction zone for Li–O_2 batteries. *Sci. Rep.* **4**, 7127; DOI:10.1038/srep07127 (2014).